Supporting Information

Hsu and Mitragotri 10.1073/pnas.1016152108

SI Materials and Methods

Phage Display. Phage library (2×10^{11} pfu, 10 μL) in 1 mL of PBS (pH 7.4) was placed in the donor compartment of the Franz diffusion cells (FDC). After 24 h, the liquid in the receiver compartment was removed and titered by adding an aliquot of the receiver solution to 200 μL of *Escherichia coli* strain ER2738 (New England Biolabs) and plating on IPTG/Xgal plates. The number of blue plaques formed after incubation for 18 h at 37 °C was counted and 20 plaques were randomly selected for sequencing. For subsequent screening rounds, 1 mL of the receiver solution was added to 20 mL of a 1:100 diluted overnight culture of ER2738 and grown for 4.5 h to amplify the phage. The phage were purified by PEG/NaCl precipitation and resuspended in PBS. The amplified phage were then used in the next round of screening. The number of phage placed in the donor compartment, 2×10^{11} pfu, was held constant for all 5 rounds of screening.

Phage Permeation. Permeability of various phage samples including phage with no peptide library, the entire phage library, skin penetrating and cell entering (SPACE)-peptide displaying phage and heptaglycine phage was determined following the same procedure described above (without the amplification and follow-up screening steps) using the number of phage colonies detected in the receiver samples and standard equations for determining permeability.

Dermis Screen. For the dermis screen, the phage display library was also placed in the donor compartment of the FDC. After 24 h, the liquid from the donor compartment was removed and the skin was placed at 60 °C for 90 s. The epidermis was then removed from the dermis. To extract phage from the dermis, the dermis was cut up into small pieces and then homogenized (IKA disperser). The homogenate was spun down at 5,000 rpm for 5 min and then resuspended in PBS and incubated at room temperature for 5 min. The samples were then centrifuged again and washed two more times. After the final centrifuge spin, the homogenates were resuspended in 1% NP40 (Sigma) to elute the remaining phage from the dermis. The eluate was then plated and amplified according to the methods listed above. This cycle was repeated for a total of five rounds. At the end of the fifth round of screening, about 1.9×10^5 phage were recovered from the dermis. Phage were sequenced and the three leading sequences in the fifth round were AC-KTGSHNQ-CG (30%), AC-MGPSSML-CG (30%), and AC-TDPNQLQ-CG (20%).

Phage Cloning. Phage displaying specific sequences were cloned (M13KE vector, New England Biolabs). The peptide sequence was inserted in between the KpnI and EagI restriction sites. To differentiate the original M13KE vector from the modified M13KE vector containing the peptide insert, the reverse primer was engineered to modify the EagI restriction site (5′-CGGCCG-3′) to the SacII restriction site (5′-CCGCGG-3′) through two site mutations. Both the forward and reverse primers were used to replicate the entire vector. The forward primer was 5′-GTTCCGCGGAAACTGTTGAAAGTTGTTTAGCAAAATCCC-3′. The reverse primer for TGSTQHQ and THGQTQS were 5′-TTTCCGCGGAACCTCCACCGCACTGATGCTGCTCGAACCAGTACAAGCAGAGTGAGAATAGAAAGGTACTACTAAAGGAATTGCGAATAATAATTTTTTCAC-3′ and 5′-TTTCCGCGGAACCTCCACCGCA(AGACTGAGTCTGCCCATGAGT)ACAAGCAGAGTGAGAATAGAAAGGTACTACTAAAGGAATTGCGAATAATAATTTTTTCAC-3′, respectively.

The replication products were purified and then digested with SacII to produce the blunt ends required for ligation of the vector. The modified vector was electroporated into electrocompetent ER2738 cells and then immediately placed in 1 mL of super optimal broth with catabolite repression medium (New England Biolabs) and grown for 45 min at 37 °C. The resulting culture was then placed into 50 mL of a 1:100 diluted overnight culture and grown for 4.5 h. The amplified phage were purified using the protocol stated above and titered. Plaques were picked after 18 h and sequenced to verify the peptide being displayed on the phage surface.

Fluorescent Labeling of Phage. Phage particles were labeled using the Alexa Fluor 488 protein labeling kit (Invitrogen). The Alexa Fluor 488 contains a tetrafluorophenyl ester which reacts with the primary amine groups on the coat proteins of the phage. 2×10^{12} pfu in deionized (DI) water or PBS were added to DI water to obtain a total volume of 500 μL. The phage solution was then added to 50 μL of 1 M sodium bicarbonate and the resulting solution was placed into a vial containing the fluorescent dye and was at room temperature for 1 h. The phage were then purified with PEG/NaCl to remove the excess unreacted dye and titered. To resemble the phage screening experiments, 2×10^{11} pfu was added to the donor compartment of the FDC and the skin samples were harvested after 24 h for imaging.

Macromolecule Penetration in Porcine Skin. To conjugate the peptide to the macromolecule streptavidin, 80 μL of a 1 mg/mL biotinylated peptide solution was incubated with 20 μL of a 2 mg/mL streptavidin-Alexa Fluor 488 conjugate (Invitrogen) solution and incubated at room temperature for 30 min. The resulting solution was then placed into the donor compartment of the FDC. For the delivery of quantum dots into the skin, 198 μL of a 100 ng/mL biotinylated peptide solution was incubated with 2 μL of QDot 525 streptavidin conjugate (Invitrogen) for 1 h at room temperature. The 200 μL suspension was then placed into the donor compartment of the FDC. All skin samples were harvested after 24 h.

Preparation of Skin Samples for Confocal Microscopy Imaging. The skin samples were placed into 4% paraformaldehyde (Electron Microscopy Sciences) overnight at 4 °C immediately after being harvested and rinsed with DI water. Skin samples were then frozen in OCT compound and sectioned at a thickness of 20 μm on a cyrotome (Leica). The tissues were mounted on slides which were positively charged to adhere the tissue to the glass slide (Fisher Scientific). The slides were washed in DI water for 5 min prior to staining with 5 μg/mL Hoechest 33342 (Invitrogen) for 5 min. The slides were then washed again in DI water for 5 min and then allowed to dry completely at room temperature in the dark. Ten microliters of Permount mounting medium (Fisher Scientific) was placed on top of the skin section along with a glass cover slip and then the slides were sealed. All samples were imaged on a confocal microscope (Leica and Olympus Fluoview 500).

Stratum Corneum (SC) Studies. To isolate the SC from full thickness skin, the skin was placed in a 60 °C water bath for 90 s. After removal from the water bath, the epidermis was separated from the dermis. The SC was then placed epidermis side down in a Petri dish containing 0.25% trpysin to remove the epidermis from

the SC. The SC was washed in DI water and then allowed to dry completely at room temperature. To delipidize the SC, the SC was placed in the following chloroform:methanol solvent mixtures: 2:1 (vol/vol), 1:1 (vol/vol), and 1:2 (vol/vol) for 15 min each. To confirm the removal of lipids, FTIR was performed on the SC samples before and after exposure to the solvent mixtures.

FTIR Spectroscopy of SC. FTIR was performed on SC samples to see the effects different peptide solutions had on the SC structure. SC was cut into 1.5 × 1.5 cm pieces and a control spectrum was obtained for each piece prior to exposure with peptide. Two milliliters of a peptide solution was then incubated with the SC for 24 h. The SC samples were then rinsed with DI water and allowed to completely dry at room temperature. The spectra were read again for each SC sample and the before and after spectra were compared to determine the effect each peptide had on SC structure. Spectra were obtained using a Nicolet Magna 850 spectrometer with a resolution of 2 cm^{-1} and averaged over 400 scans.

Cell Culturing Conditions. Human adult epidermal keratinocytes (Invitrogen) were cultured in EpiLife Medium (Invitrogen) supplemented with Human Keratinocyte Growth Supplement (Invitrogen), human skin fibroblasts [American Type Culture Collection (ATCC)] were cultured in Dulbecco's modified Eagle's medium (ATCC) supplemented with 10% fetal bovine serum, pooled human umbilical vein endothelial cells (HUVEC, Lonza) were cultured in M199 medium on 1% gelatin-coated flasks supplemented with 15% fetal bovine serum, 15 μg/mL endothelial cell growth supplement, 100 μg/mL heparin, and 2 mM L-glutamine, and MDA-MB-231 breast cancer cells were cultured in Dulbecco's modified Eagle's medium (ATCC) supplemented with 10% fetal bovine serum. All cell culture media were supplemented with 100 U/mL pencillin and 100 μg/mL streptomycin and cultures were grown under standard cell culture conditions (37 °C with 5% CO_2).

Preparation of Cell Culture Samples for Confocal Microscopy Imaging. After incubation, cells were washed with HBSS (Lonza) and incubated with 1% trypan blue for 5 min to quench any fluorescence on the surface of the cell. The cells were then fixed with 4% paraformaldehyde for 3 min and again washed in HBSS. The cells were then incubated with Hoechest 33342 (5 μg/mL) for 5 min and then washed in HBSS. The cell culture dishes were then filled with HBSS and imaged using confocal microscopy (Olympus Fluoview 500).

Endocytosis Inhibitors. Endocytosis inhibitors were incubated with human keratinocytes prior to addition of fluorescently labeled control and SPACE peptide. The endocytosis inhibitors used were 5-(*N*-ethyl-*N*-isopropyl)amiloride (EIPA) (Invitrogen) and chlorpromazine, nystatin, and deoxy-D-glucose (Sigma). EIPA was dissolved in DMSO and used at a concentration of 100 μM. Chlorpromazine, nystatin, and deoxy-D-glucose were dissolved in sterile water and used at the concentrations of 10 μg/mL, 25 μg/mL, and 5 mM, respectively.

Preparation of Samples for Flow Cytometry. After incubation with fluorescently labeled peptide, the media was removed and cells were washed three times for 5 min each in HBSS to remove residual fluorescence. Trypsin (0.25%, HyClone) was used to remove the cells from the cell culture plate. The cells were then centrifuged at 5,000 rpm for 5 min to pellet the cells. The cell pellet was resuspended in PBS, pH 7.4 on ice and samples were analyzed using the FACSAria flow cytometer.

Conjugation of Peptide to siRNA. A 10 mM peptide solution was incubated with a 10 mM solution of *N*-(3-Dimethylaminopropyl)-*N′*-ethylcarbodiimide hydrochloride (EDAC, Sigma) and a 9.5 mM solution of N-Hydroxysulfosuccinimide sodium salt (NHS, Sigma) in equal parts in MES buffer (pH 5.5) for 15 min. The amine modified siRNA was then added to the mixture to conjugate the peptide to siRNA and allowed to mix overnight.

Mathematical Model. Diffusion through intercellular lipids represents the classical mechanism for transdermal permeation of molecules. This mechanism, however, is generally limited to small, lipophilic molecules such as nicotine and fentanyl. Permeation of large, hydrophilic molecules is relatively less studied. Nonetheless, an increasing number of studies have reported and discussed transdermal permeation of hydrophilic macromolecules such as inulin (5 kDa) and dextran (70 kDa). Transdermal transport of such solutes is attributed to two pathways; (*i*) polar or porous pathways and (*ii*) appendages (follicles). Mathematical models have been developed to describe contributions of both pathways. Below, we extend these models to phage.

Basics of these models have already been published (1, 2) and a summary of these models is provided below. These models have been applied to describe transport of large molecules such as dextran, (hydrodynamic radius of 2.6 nm), which though smaller than the radius of the phage (~4 nm), is of the same order of magnitude. The following analysis is based on extrapolation of these models and provides informative context for interpreting phage permeation through skin.

Polar pathway. Polar (or porous) pathways have been used to describe transdermal diffusion of several hydrophilic solutes including macromolecules (1, 3–10). To cross the SC, hydrophilic solutes need to penetrate multiple lipid bilayers. However, given the low permeabilities of hydrophilic solutes across lipid bilayers, it appears unlikely that hydrophilic molecules can diffuse across the SC by the classical partition-diffusion process that plays an important role for hydrophobic solutes. Transdermal penetration of such solutes has been proposed to take place primarily through defects in the SC that exist in various physical forms including grain boundaries, fault-dislocations, nanoscale pinholes, or other abnormalities in skin structure. Hydration of the SC may further increase the occurrence of such defects. The precise size of these defects depends on the type of defect and may span a length scale of 1–100 nm.

A general expression for the permeability coefficient, K_P^{pore}, of a hydrophilic permeant diffusing through skin is given by the porous pathway as follows:

$$K_P^{\text{pore}} = \frac{\varepsilon D^{\infty}}{\tau L}\left[\int_0^{\infty} \gamma(r) H(\lambda) dr\right], \qquad \textbf{[S1]}$$

where ε, τ, and L are the porosity, tortuosity, and thickness of the membrane, respectively, and D^{∞} is the solute diffusion coefficient in infinite dilution. $H(\lambda)$ is the steric hindrance factor, where λ is the ratio of the hydrodynamic radius of the permeant, r_h, and the effective pore radius of the skin, r (that is, $\lambda = r_h/r$). The relationship between $H(\lambda)$ and λ is given by the hindered transport theory and is described in the literature (11). The pore size distribution, $\gamma(r)$, in skin has been described for porcine skin by the following function (4):

$$\gamma(r) = 0.024 \exp(-0.00045 r^2). \qquad \textbf{[S2]}$$

To put Eq. **S2** in perspective, consider the energetics of pore (or void) formation in a medium, for example skin. The probability of pore formation can be related to the free energy of pore formation according to the following general equation:

$$\text{probability} \propto \exp\left(-\frac{\pi r^2 E}{kT}\right), \qquad \textbf{[S3]}$$

where E is the free energy of pore formation per unit area per unit pore. A comparison of Eq. **S2** and **S3** indicates that the value of E for a pore with a 4 nm radius in porcine skin is $<1kT$, a value that is relatively small.

Values of ε for porcine skin have been determined to be about 2×10^{-5} (4). Similarly, tortuosity, τ, for diffusion of large hydrophilic solutes in porcine SC has been shown to be approximately 1 (4). D_p^{∞} is the solute diffusion coefficient in water and has been calculated using correlations such as the Wilke–Chang or Stoke–Einstein equation, as follows:

$$D_p^{\infty} = \frac{2.6 \times 10^{-5}}{r_h}, \qquad \textbf{[S4]}$$

where r_h is in angstrom and D_p^{∞} is in cm^2/s. By combining Eqs. **S1**, **S2**, and **S4**, we estimate the contribution of porous pathways for a solute of radius r_h, as follows:

$$K_P^{\text{pore}}(r_h) = \frac{1.3x10^{-3}}{r_h} \int_{r_h}^{\infty} H(\lambda)\gamma(r)dr, \qquad \textbf{[S5]}$$

where K_P^{pore} is in cm/h. By substituting $r_h = 40$ Å (corresponding to radius of phage), one gets $K_P^{\text{pore}}(r_h) \sim 10^{-8}$ cm/h.

Contribution of appendages. Large solutes may also be able to diffuse across the skin through appendages. Although the density of hair follicles varies substantially with anatomical location, the average density of hair follicles in porcine skin is estimated to be approximately 10 per cm^2. A large fraction of the follicle, however, is occupied by the hair and is not available for transport. The contribution of shunts to skin permeability is given by the following:

$$K_P^{\text{shunt}} = \frac{\phi_s D_s}{L_{\text{shunt}}}, \qquad \textbf{[S6]}$$

where ϕ_s is the fraction of skin area occupied by follicles that is available for transport, D_s is the solute diffusion coefficient in the contents within the follicles, and L_{shunt} is the diffusion path length through follicles. The area fraction of skin in the follicle that is available for transport is $\sim 10^{-4}$ cm^2/cm^2. D_s can be estimated using the Wilke–Change equation or the Stoke–Einstein relationship. Assuming the follicles are filled with a viscous liquid and given the large size of the phage, D_s can be approximated to be $\sim 10^{-8}$ cm^2/s. L_{shunt} is approximately 500 μm. By substituting the above values for ϕ_s and L_{shunt} one can obtain the following expression for $K_P^{\text{shunt}} \sim 10^{-7}$ cm/h.

The above equations therefore estimate that phage permeability across porcine skin in the range of 10^{-7} to 10^{-8} cm/h.

To compare these estimates with experimental data, we measured phage permeation across porcine skin (see methods described above). Control phage (phage without any peptide displayed) exhibited a permeability $\sim 10^{-9}$ cm/h. Phage that displays heptaglycine also exhibited a low permeability of $\sim 10^{-10}$ cm/h. The entire phage display library exhibited a permeability of $\sim 10^{-8}$ to 10^{-7} cm/h and the permeability of phage displaying the SPACE sequence was 10^{-7} to 10^{-6} cm/h. These numbers are generally consistent with theoretical predictions. Note that the measured permeabilities may not represent steady-state values and may not fulfill the classical definition of permeability; nonetheless, these numbers provide reasonable values to allow comparisons with theoretical predictions.

Given that all phage particles used in this study were of identical size, the likely explanation for higher permeability of SPACE phage over control phage (no peptide displayed) is due to the peptide displayed on the surface of the phage. The porous pathway model assumes that partitioning of solutes in the skin is unity, that is, the solute exhibits no affinity toward the skin. If SPACE phage were to exhibit higher affinity toward the skin, it would lead to higher portioning and penetration of phage across the skin. Experimental observations indeed suggest that SPACE increases the affinity of the cargo toward skin components, especially keratin. Hence, we hypothesize that this increased affinity is the primary reason behind increased penetration of SPACE phage over control phage.

To further confirm this hypothesis, we conducted experiments where the effect of excess SPACE peptide on permeation of SPACE phage across porcine skin was assessed. Specifically, SPACE sequence-displaying phage was placed on the skin in presence of about a 100,000-fold excess SPACE peptide ($\sim 10^5$ free SPACE peptides per SPACE peptide on phage). Excess SPACE peptide significantly reduced permeation of SPACE phage and the permeability of SPACE-phage phage in this case was close to heptaglycine phage ($\sim 10^{-10}$ cm/h).

1. Tang H, Mitragotri S, Blankschtein D, Langer R (2001) Theoretical description of transdermal transport of hydrophilic permeants: Application to low-frequency sonophoresis. *J Pharm Sci* 90(5):545–568.
2. Peck KD, Ghanem AH, Higuchi WI (1994) Hindered diffusion of polar molecules through and effective pore radii estimates of intact and ethanol treated human epidermal membrane. *Pharm Res* 11:1306–1314.
3. Mitragotri S, et al. (2011) Mathematical models of skin permeability: An overview. *Int J Pharm* doi: 10.1016/j.ijpharm.2011.02.023.
4. Tezel A, Sens A, Mitragotri S (2003) Description of transdermal transport of hydrophilic solutes during low-frequency sonophoresis based on a modified porous pathway model. *J Pharm Sci* 92:381–393.
5. Tezel A, Sens A, Mitragotri S (2002) A theoretical analysis of low-frequency sonophoresis: Dependence of transdermal transport pathways on frequency and energy density. *Pharm Res* 19:1841–1846.
6. Tezel A, Mitragotri S (2003) On the origin of size-dependent tortuosity for permeation of hydrophilic solutes across the stratum corneum. *J Controlled Release* 86:183–186.
7. Polat BE, Seto JE, Blankschtein D, Langer R (2011) Application of the aqueous porous pathway model to quantify the effect of sodium lauryl sulfate on ultrasound-induced skin structural perturbation. *J Pharm Sci* 100:1387–1397.
8. Seto JE, Polat BE, Lopez RF, Blankschtein D, Langer R (2010) Effects of ultrasound and sodium lauryl sulfate on the transdermal delivery of hydrophilic permeants: Comparative in vitro studies with full-thickness and split-thickness pig and human skin. *J Controlled Release* 145:26–32.
9. Tang H, Blankschtein D, Langer R (2002) Prediction of steady-state skin permeabilities of polar and nonpolar permeants across excised pig skin based on measurements of transient diffusion: Characterization of hydration effects on the skin porous pathway. *J Pharm Sci* 91:1891–1907.
10. Tang H, Blankschtein D, Langer R (2002) Effects of low-frequency ultrasound on the transdermal permeation of mannitol: Comparative studies with in vivo and in vitro skin. *J Pharm Sci* 91:1776–1794.
11. Deen WM (1987) Hindered transport of large molecules in liquid-filled pores. *AIChE Journal* 33:1409–1425.

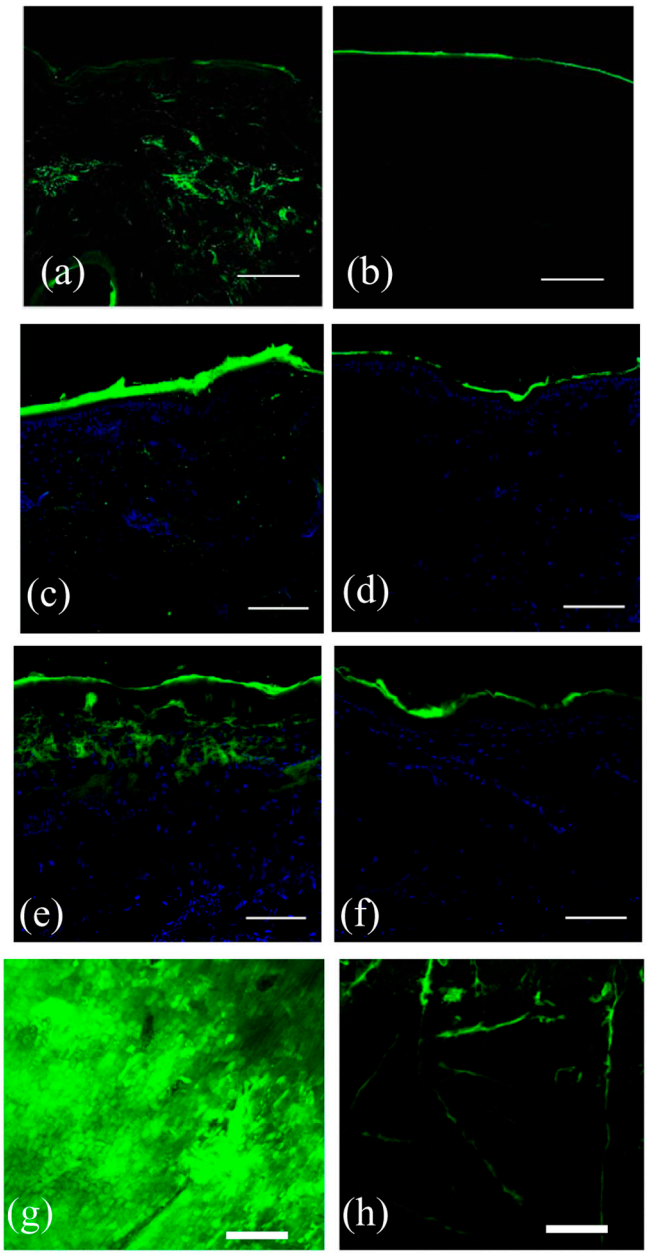

Fig. S1. Skin penetration of fluorescently labeled molecules through skin. (*A* and *B*) Penetration of fluorescently labeled phage displaying peptides into porcine skin. (*C* and *D*) Penetration of biotinylated peptide-streptavidin coated quantum dots into porcine skin. (*E* and *F*) Penetration of fluorescently labeled peptide into human skin. (*G* and *H*) Top view (looking down on SC) of fluorescently labeled peptide in human skin. *A*, *C*, *E*, and *G* represent images of SPACE peptide and *B*, *D*, *F*, and *H* represent images of control peptide. Scale bar: 200 μm.

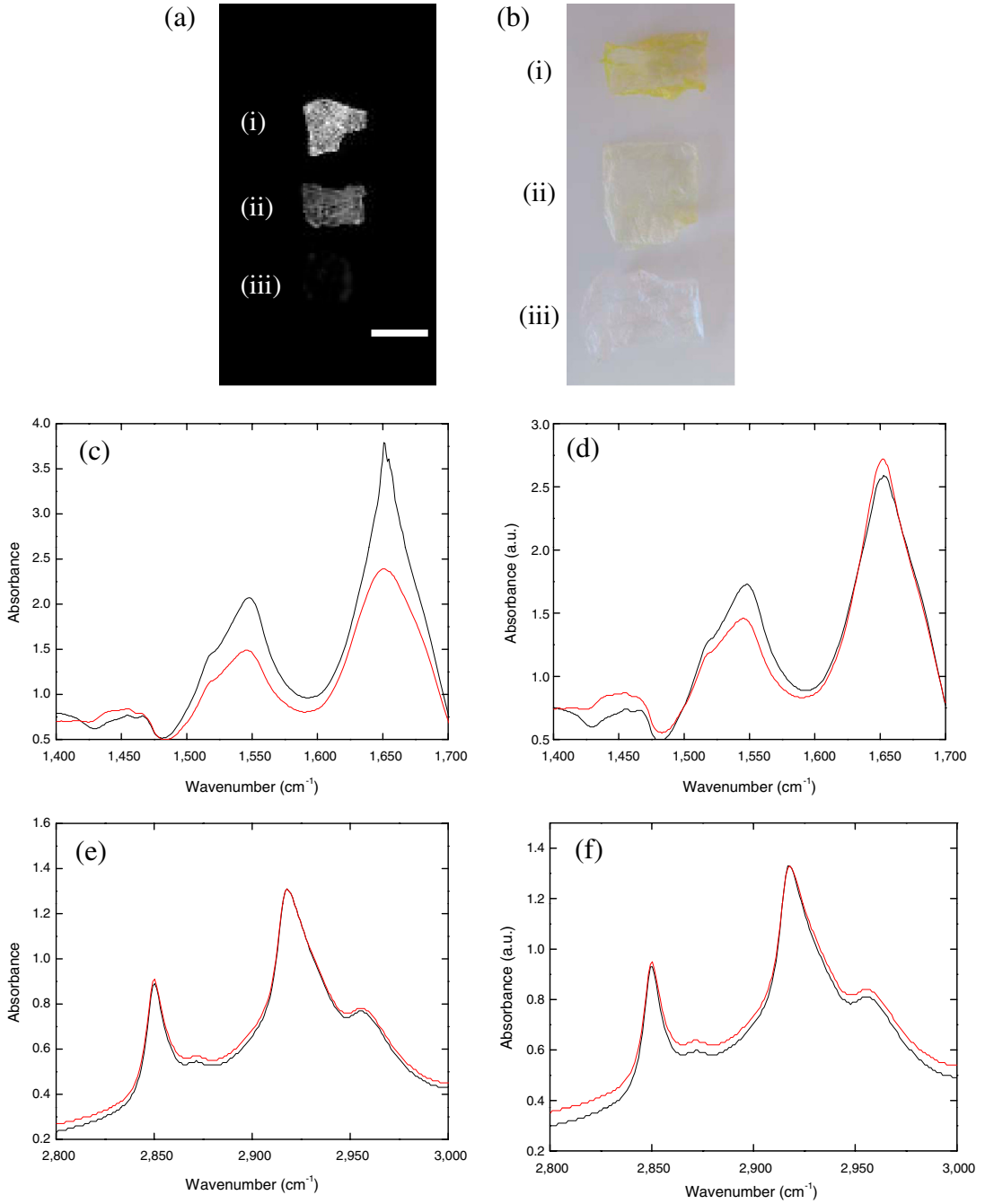

Fig. S2. (*A*–*B*) Binding of fluorescently labeled peptide to delipidized SC. Images of delipidized SC under UV (*A*) and visible light (different samples) (*B*). *A* (i–iii) and *B* (i–iii) represent the SPACE peptide, control peptide, and no peptide, respectively. Scale bar: 1 cm. Note that the SC samples shown above were delipidized to ensure a comparison of binding ability and not transport ability of the peptides. Hence, the difference between the control and SPACE peptide as seen above may not directly translate to their effect on skin penetration. (*C*–*F*) FTIR spectra of SC before and after treatment with peptide. (*C* and *D*) The region of spectra 1,400–1,700 cm^{-1} for the SPACE peptide and control peptide, respectively. (*E* and *F*) The region of spectra 2,800–3,000 cm^{-1} for the SPACE peptide and control peptide, respectively. Initial spectra and final spectra are indicated in black and red, respectively.

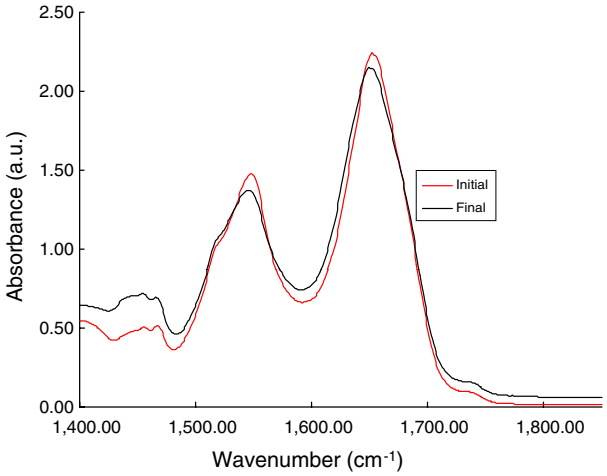

Fig. S3. FTIR spectra of amide I and amide II region for SC before and after treatment with no peptide.

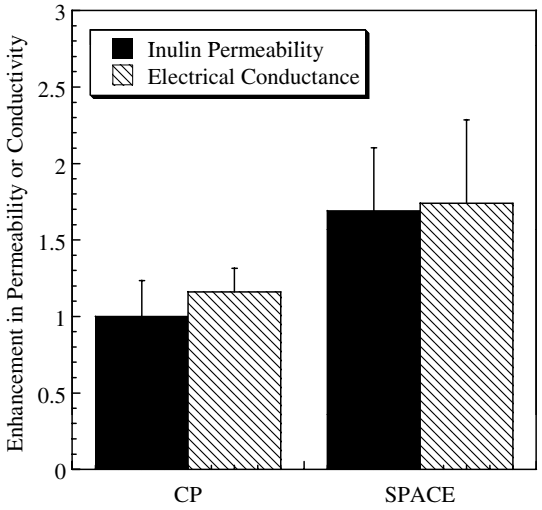

Fig. S4. Inulin permeability and the electrical conductivity enhancement of porcine skin after coincubation with control peptide (CP) and SPACE peptide.

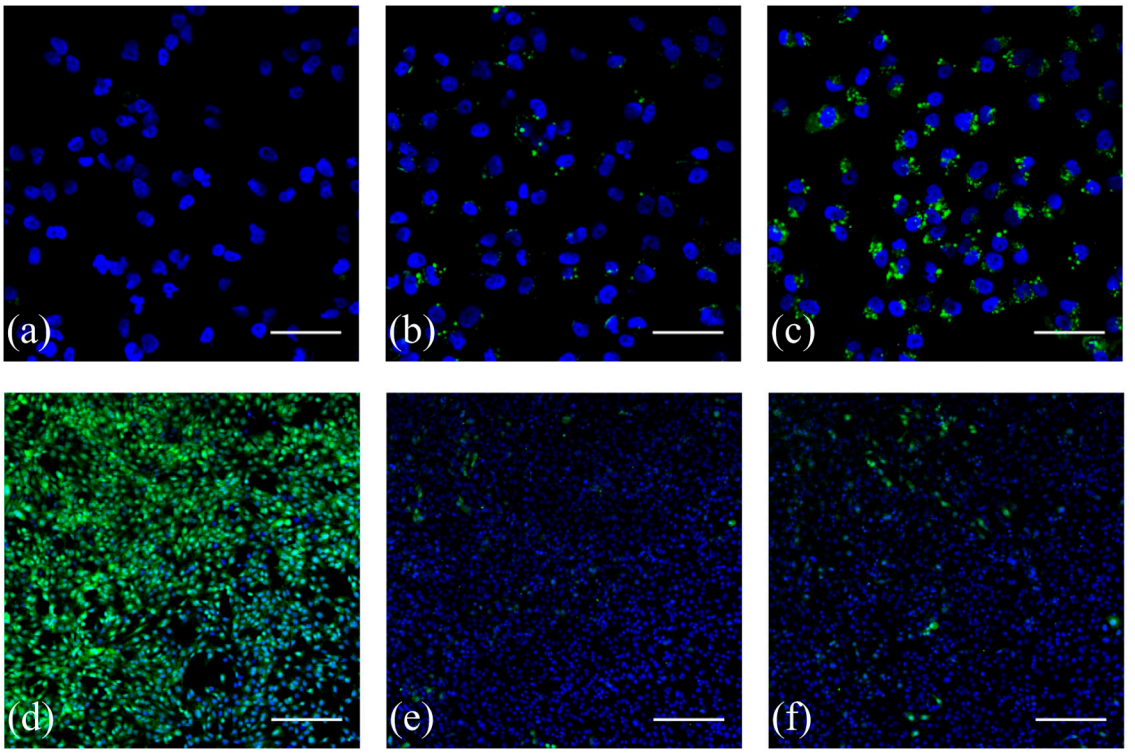

Fig. S5. (*A–C*) Penetration of fluorescently labeled peptide into MDA-MB-231 human breast cancer cells after 6 h. Images of cells with no peptide (*A*), control peptide (*B*), and SPACE peptide (*C*). Scale bar: 50 μm. (*D–F*) Confocal images of GFP-expressing endothelial cells after treatment with GFP siRNA complexed with Lipofectamine. (*D*) Treatment of cells with Lipofectamine only (no siRNA), (*E*) with Lipofectamine complexed with GFP siRNA, and (*F*) with Lipofectamine complexed with SPACE-GFP siRNA. Scale bar: 200 μm.

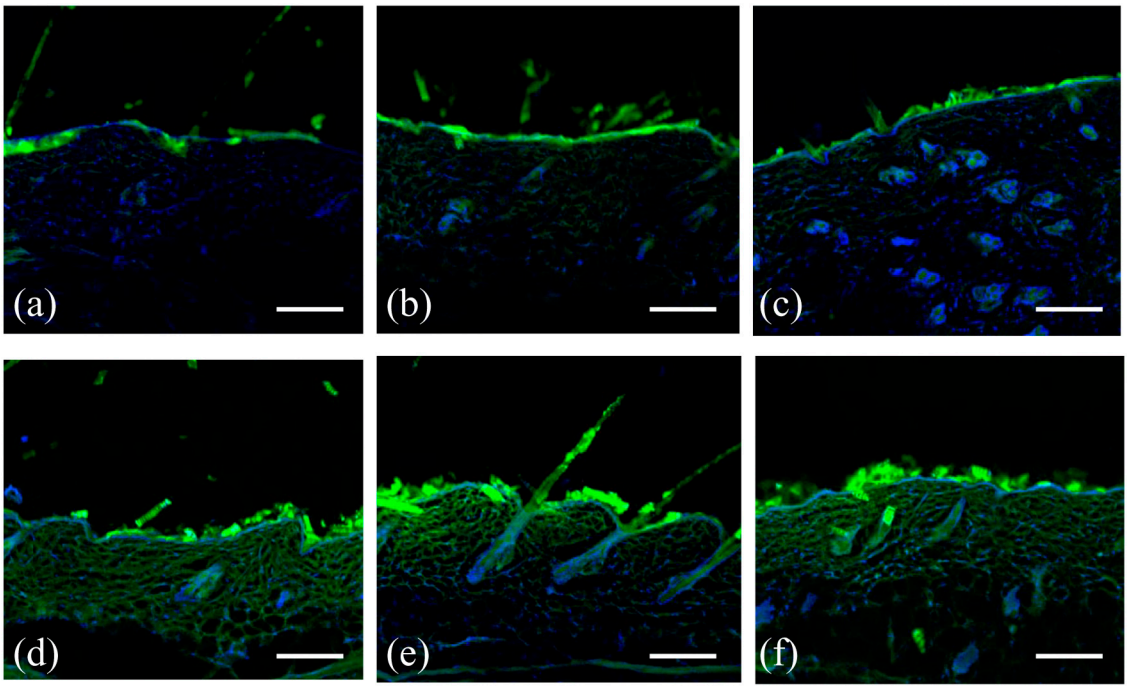

Fig. S6. Penetration of fluorescently labeled peptide into mouse skin in vivo after 30 min. Three representative images are provided for each case. (*A–C*) Penetration of fluorescently labeled control peptide and (*D–F*) fluorescently labeled SPACE peptide. Scale bar: 50 μm.

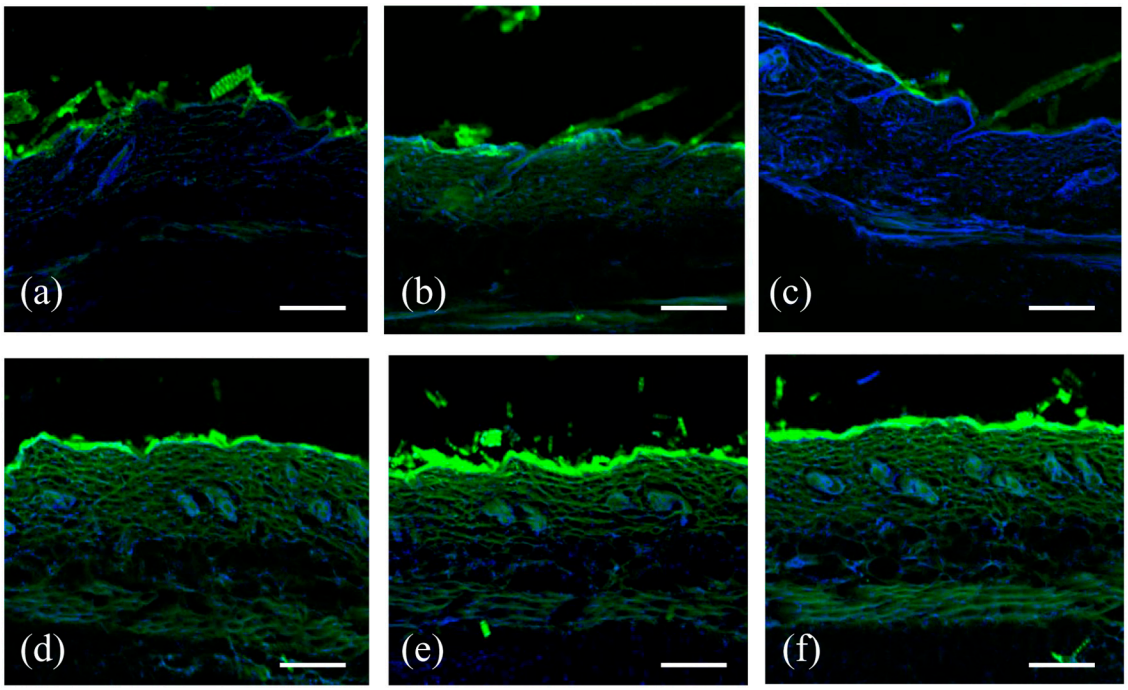

Fig. S7. Penetration of fluorescently labeled peptide into mouse skin in vivo after 2 h. Three representative images are provided for each case. (*A–C*) Penetration of fluorescently labeled control peptide and (*D–F*) fluorescently labeled SPACE peptide. Scale bar: 50 μm.

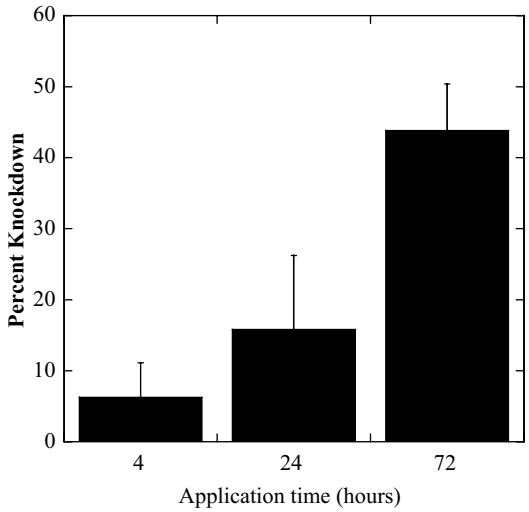

Fig. S8. GAPDH knockdown at various application times. The reduction in GAPDH protein levels after SPACE-GAPDH siRNA application times of 4, 24, and 72 h.